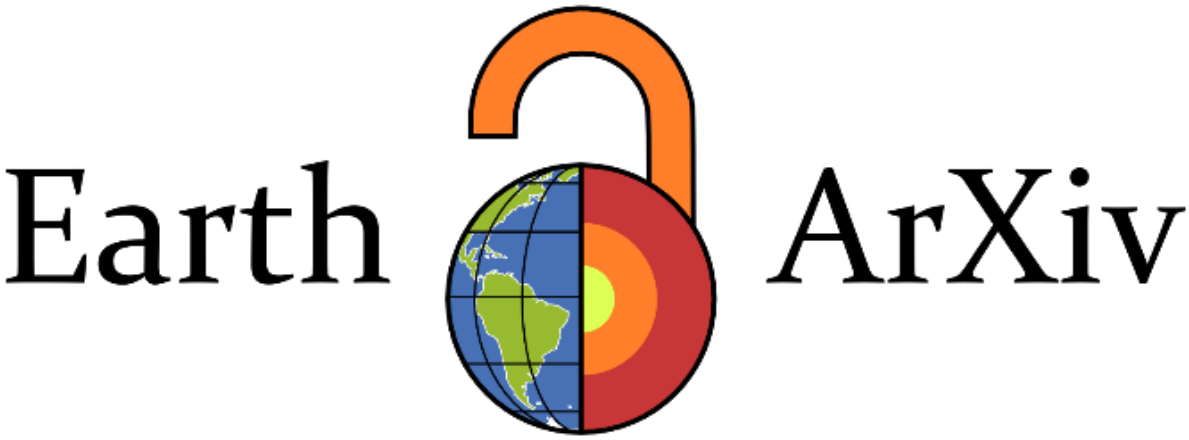

Cooling after net zero

Nathaniel Tarshish[1*], Nadir Jeevanjee[2] and Inez Fung[3]

[1*]Center for the Environment, Harvard University, Cambridge, MA, USA.
[2]Geophysical Fluid Dynamics Laboratory, Princeton, NJ, USA.
[3]Department of Earth and Planetary Science, University of California, Berkeley, CA, USA.

*Corresponding author(s). E-mail(s): ntarshish@g.harvard.edu;
Contributing authors: nadir.jeevanjee@noaa.gov; ifung@berkeley.edu;

Abstract

Climate policy aims to limit global warming by achieving net-zero greenhouse gas emissions. Climate models indicate that achieving net-zero emissions yields a nearly constant global temperature over the following decades. However, whether temperatures remain stable in the *centuries* after net-zero emissions is uncertain, as models produce conflicting results. Here, we explain how this disagreement arises from differing estimates of two key climate metrics, which govern the carbon system's disequilibrium and the ocean's thermodynamic disequilibrium, respectively. By constraining these metrics using multiple lines of evidence, we demonstrate—with greater than 95% confidence—that global temperature anomalies decline after net-zero. In the centuries that follow net-zero, the global-mean temperature anomaly is projected to decrease by 40% (median estimate). Consequently, achieving net-zero emissions very likely halts further temperature rise, even on multi-century timescales.

Keywords: committed warming, net zero, zero emissions, temperature

Introduction

The Paris Agreement seeks to stabilize global temperatures by achieving net-zero greenhouse gas (GHG) emissions [1]. This net-zero strategy emerged just a few years before the agreement, spurred by recent research suggesting that emissions must be almost entirely eliminated to prevent further warming [2–4]. Earlier policies focused instead on stabilizing atmospheric GHG *concentrations*, allowing net-positive emissions that were offset by carbon uptake from land and oceans [5].

With stabilized GHG concentrations, however, surface temperatures still continue to rise. This surface warming is governed by both the *source* of heat—radiative forcing from GHGs—and by the *sinks* of heat—mixing with the cold, deep ocean and radiative cooling to space. Over time, the deep ocean warms, weakening the deep-ocean heat sink and thus increasing surface temperatures. Therefore, simply stabilizing GHG concentrations does not counteract the diminishing ocean heat sink. To stabilize the temperature, then, it is necessary for the heat source (i.e., the radiative forcing) to decline as well.

Does the cessation of emissions, which enables natural land and ocean carbon sinks to lower atmospheric CO_2 concentrations, reduce the heat source enough to stop warming? This question has been extensively studied with climate models [2, 4, 6–11], which generally find that zeroing emissions indeed halts the rapid rise in temperature rise observed over the historical period. Therefore, future warming appears to be mainly due to future emissions.

Given the significant challenges in eliminating GHG emissions entirely, policies aim to stabilize the temperature with net-zero, rather than zero, emissions [3, 12]. Net-zero emissions involve offsetting positive GHG emissions with negative CO_2 emissions, i.e., deliberate removal of CO_2 from the atmosphere. It is generally assumed that the long-term temperature responses to zero and net-zero emissions are similar (we confirm this below, and in fact find that the former generally provides an upper bound on the latter). This similarity, along

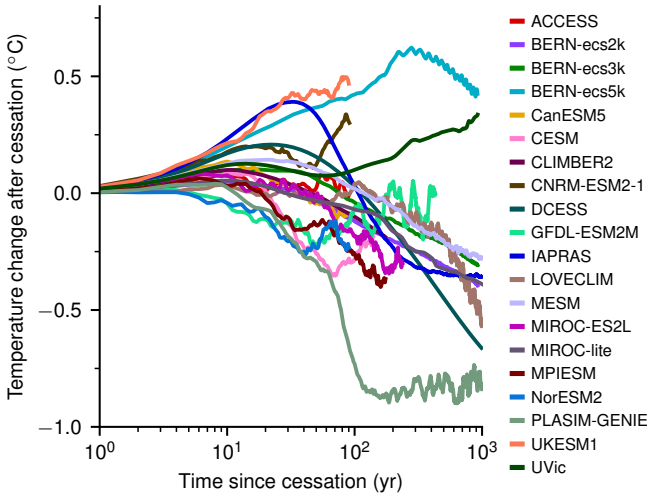

Fig. 1 Model responses to emissions cessation diverge over time. Post-emissions temperature change in ZECMIP models [10] driven by a 1%/yr increase in CO_2 concentration until diagnosed cumulative emissions reach 1000 GtC. Plot is reproduced from Figure 3b of ref. [10] with a logarithmic x-axis to emphasize inter-model divergence over time.

with the relative simplicity of zero emissions scenarios, have made the zero-emissions response a useful tool for understanding climate stabilization [13]. In its Sixth Assessment Report (AR6), the Intergovernmental Panel on Climate Change (IPCC) assessed that the global-mean surface temperature change over the fifty years following a complete cessation of emissions is only -0.1 ± 0.2°C [Section 4.7.1 11].

This IPCC assessment was based on ZECMIP, a recent intercomparison of roughly two dozen models which explored the temperature change after emissions cease, known as the Zero Emissions Committment (ZEC) [7, 10]. As shown in Figure 1, the ZECMIP ensemble exhibits little temperature change in the first few decades following emissions cessation. However, over subsequent *centuries*, simulations diverge, with models projecting a multi-century spread exceeding 1°C. Thus, while emissions cessation may halt rapid warming in the near term, ZECMIP suggests that prolonged, slow warming on oceanic timescales cannot be ruled out. Uncertainty in long-term ZEC is perhaps unsurprising, given substantial inter-model differences in fundamental climate parameters and processes. However, ZEC appears only weakly correlated with standard metrics of climate sensitivity [10], leaving much of the variance in Figure 1 unexplained (Supplementary Fig. 1).

This uncertainty in the determinants of ZEC complicates efforts to maintain global temperatures below a target value in the coming centuries [13]. Achieving temperature targets involves limiting cumulative emissions to a prescribed total referred to as the "carbon budget" [3, 14]. If warming persists even after net zero, the carbon budget must be tightened [15]. Given the uncertainty surrounding long-term ZEC, the IPCC assessed with *very low confidence* that the AR6 carbon budgets guarantee climate stability beyond the 21st century [16, Section 5.5.2.3].

Here, we aim to address this lack of confidence by bringing the long-term implications of net-zero into sharper focus. By appealing to a simple energy balance model, we explain how the ZECMIP model divergence in Fig. 1 is explained by differing estimates of two key quantities: the forcing and thermal disequilibria at the time of zero emissions. When these underlying disequilibria are constrained by multiple lines of evidence, and made consistent with AR6 integrated assessments, the simple model robustly predicts multi-century cooling after net-zero GHG emissions. This finding suggests that achieving net-zero halts temperature rise not only this decade, but for centuries to come.

Climate dynamics after net zero

We define the long-term ZEC [7] as the difference between the "final" temperature anomaly T_f and the temperature anomaly at the time emissions cease T_ze,

$$\mathrm{ZEC} = T_\mathrm{f} - T_\mathrm{ze}\,. \tag{1}$$

Anomalies are taken with respect to preindustrial, and final refers to the quasi-equilibrium climate state that emerges after many centuries of ocean overturning have equilibrated atmospheric and oceanic carbon and heat. We approximate this equilibrium with the simulation results a thousand years after cessation.

Consider the magnitude of ZEC relative to the temperature anomaly at cessation,

$$\frac{\text{ZEC}}{T_{\text{ze}}} = \frac{T_{\text{f}}}{T_{\text{ze}}} - 1\,. \tag{2}$$

In the final state, by definition, $T_{\text{f}} = F_{\text{f}}/\lambda$, where F_{f} is the final radiative forcing and λ is the equilibrium climate feedback parameter. Let $\tilde{T} = F_{\text{ze}}/\lambda$ be the hypothetical temperature that would arise if the climate were in thermal equilibrium with the forcing *at emissions cessation*. Substitution yields

$$\frac{\text{ZEC}}{T_{ze}} \approx \frac{F_{\text{f}}/F_{\text{ze}}}{T_{\text{ze}}/\tilde{T}} - 1\,. \tag{3}$$

The ratio $F_{\text{f}}/F_{\text{ze}}$ represents the *forcing* disequilibrium at cessation, due to (primarily short-lived) non-CO_2 species and CO_2 that is airborne at cessation but will be taken up by the ocean (or land) at equilibrium. Likewise, $T_{\text{ze}}/\tilde{T}$ quantifies the *thermal disequilibrium* due to the not-yet-warmed deep ocean.

To constrain $T_{\text{ze}}/\tilde{T}$, we appeal to the two-box model of climate [17–19]. This simple model partitions the temperature response to forcing into two timescales: $T \approx T_{\text{fast}} + T_{\text{slow}}$, where T_{fast} corresponds to a ~ 5 yr mode associated with the fast adjustment of surface ocean, and T_{slow} represents a ~ 200 yr mode associated with slow deep ocean warming [20]. When the temperature response is dominated by the fast mode, the thermal disequilibrium is approximately constant: in this state, $T(t)/\tilde{T}(t) \approx T_{\text{fast}}(t)/\tilde{T}(t) = T_{\text{fast}}(t)/\lambda^{-1}F(t)$, and, given the fast mode's limited memory, $T_{\text{fast}}(t)$ is largely determined by the current forcing $F(t)$. In fact, to first order we have $T_{\text{fast}}(t) \propto F(t)$, fixing $T_{\text{fast}}(t)/\lambda^{-1}F(t)$ to a constant. (See Methods for a more complete derivation.)

The value of this constant thermal disequilibrium can be computed from any scenario in which the temperature response is dominated by the fast mode. To make contact with established metrics, we compute the fast-mode's disequilibrium in the standard 1%/yr increase in CO_2 scenario [21, 22]. The temperature response at the time of CO_2 doubling (year 70) is the transient climate response: $\text{TCR} \approx T_{\text{fast}}(70\,\text{yr})$. The equilibrium temperature if forcing were held constant at doubling is the equilibrium climate sensitivity, $\text{ECS} = \lambda^{-1}F_{2\times}$. Therefore, the fast-mode's disequilibrium is TCR/ECS.

For a general scenario, as long as the zero-emissions state is dominated by the fast mode, the thermal disequilibrium is constrained to TCR/ECS, and hence

$$\frac{\text{ZEC}}{T_{ze}} \approx \frac{F_{\text{f}}/F_{\text{ze}}}{\text{TCR/ECS}} - 1\,. \tag{4}$$

Given the extensive literature constraining TCR and ECS with multiple lines of evidence [23, 24], the above formula connects the post-emissions response to our broader understanding of climate change. The formula makes precise the prior observation that ZEC simulations are influenced by the degrees of disequilibrium in the carbon system and thermal response at the time of emission cessation [9, 10, 25]. Equation 4 also generalizes the related result of ref. [26], which derives an analytic expression for ZEC in the context of an idealized carbon-cycle model.

We now validate the general formula against the higher-complexity models participating in ZECMIP. We first apply the formula to experiments [10] in which the CO_2 concentration increases at a rate of 1%/yr until the diagnosed cumulative emissions reach 750, 1000, and 2000 GtC. Fig. 1 corresponds to the 1000 GtC case. For models that simulate only the first century after emissions cessation, we adapt the formula to predict ZEC at the end of the simulation, rather than at the long-term equilibrium (see Methods).

We use the ECS, TCR, and $F_{2\times}$ values reported for each model in ref. [10] and diagnose F_{ze} and F_{f} by approximating the forcing as logarithmic in the CO_2 concentration. Fig. 2 compares the formula's predictions for ZEC to the experimental values in the 1000 GtC experiment. See Supplemental Figure 8 for the 750 and 1000 GtC cases. Comparing theory to experiment across the three cases yields an average error of 0.10 and a Pearson's coefficient of $R^2 = 0.78$, building confidence that the formula generally captures the ZECMIP responses to emissions cessation.

Constraining with more evidence

Equation 4 highlights the limitations of inferring the long-term zero-emissions response from the ZECMIP results. We do not expect the TCR/ECS distribution of the ZECMIP models (an ensemble of opportunity) to be fully consistent with AR6 central estimates. In addition, $F_{\text{f}}/F_{\text{ze}}$ depends on the rate of emissions, and the

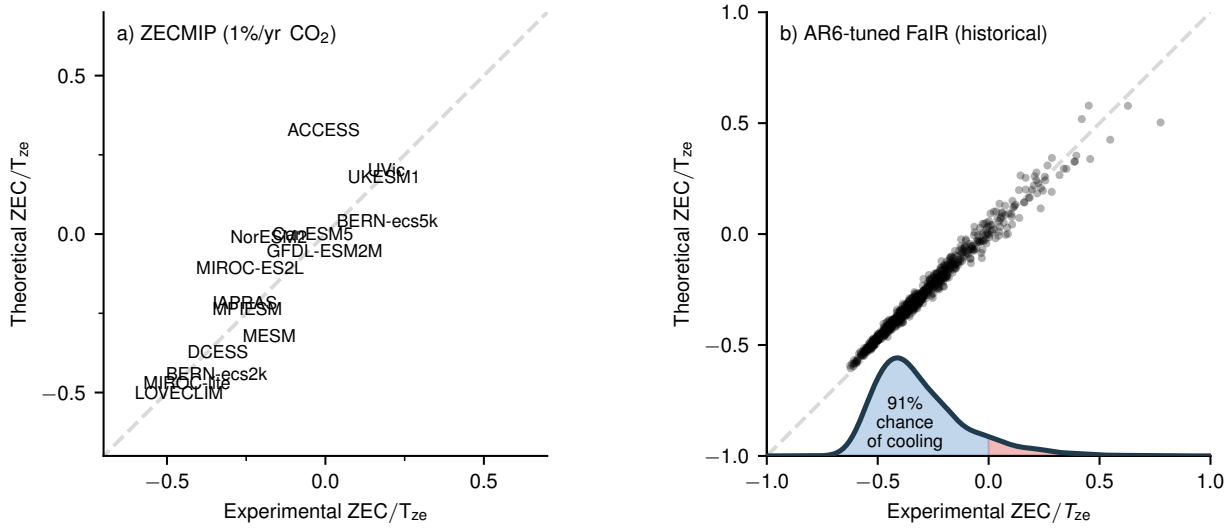

Fig. 2 Theory captures variation across models of varying complexity. Comparison between the analytic formula (Eqn. 4) and the experimental values for the fractional temperature change after emissions cessation following a 1%/yr increase in CO_2 up to 1000 GtC in the ZECMIP ensemble (a) and following historical emissions in the FaIR ensemble (b). For ZECMIP models, these results do not represent long-term committed warming, as simulations terminate before equilibrium. For the FaIR ensemble, a kernel density estimate of the ensemble's probability density function (PDF) is also shown with bandwidth set by Silverman's rule [27].

lifetime of the emitted species. Historical emissions have been notably slower and more diverse in species than the ZECMIP CO_2-only 1%/yr scenarios [28].

Here we aim to provide ZEC estimates that are consistent with historical emissions and the IPCC AR6 assessments of TCR and ECS. To begin, we consider historical ZEC (i.e., the temperature change that occurs absent future emissions). We expect that the present-day thermal disequilibrium is dominated by the fast-mode. Most of the rise in historical forcing has occurred in the last few decades [28], leaving insufficient time for the multi-century mode to react to modern forcing [18]. The absence of a substantial slow-mode contribution to present-day temperature is confirmed by climate-model simulations [18, 29] in which the forcing is abruptly zeroed and the temperature rapidly returns to near pre-industrial levels. We therefore estimate the present-day thermal disequilibrium as equal to the characteristic fast-mode value of TCR/ECS.

IPCC AR6 inferred an ECS central estimate of 3.0 K with a very likely (i.e., 5th-95th interquantile) range of [2.0-5.0] K and a TCR estimate of 1.8 [1.2-2.4] K [30, Table 7.1.13]. These assessments synthesize process-based understanding, warming over the instrumental record, paleoclimate data, and emergent constraints [23, 30]. The present-day forcing (2023 relative to 1750), in this context, F_{ze}, is estimated to be 2.8 [1.8–3.6] W/m^2 [28].

The forcing at equilibrium, F_f, is non-zero and is not assessed in AR6. Millennial simulations in ZECMIP and other studies [31] find that roughly 20% of CO2 emissions are stranded in the atmosphere on multi-century timescales, yielding $F_f \approx 1.2$ W/m^2 (see Methods). Evaluating the fractional ZEC formula (Eqn. 4) with these AR6 central estimates yields −30%. In other words, the temperature is expected to decrease by roughly 0.4 K absent future emissions. The diminishing heat *source* from declines in GHG concentrations trumps the declining heat *sink* from ocean equilibration, yielding cooling. Assessing confidence in this estimate, however, requires considering the uncertainty and covariance among the four input parameters.

To estimate these covariances (and, in the next section, to project future scenarios), we take advantage of the AR6-tuned Finite-amplitude Impulse Response (FaIR) ensemble [32]. FaIR consists of an energy balance model coupled to an idealized carbon cycle and simple analytic forcing expressions [33–35]. In AR6, the IPCC extensively relied upon FaIR for future projections, uncertainty assessment, and scenario exploration [36, 37]. Despite FaIR's reduced-complexity, the simple model can successfully emulate state-of-the-art models from the Coupled Model Intercomparison Project Phase 6 (CMIP6) and replicate historical observations [32, 34]. And, enabled by this simplicity, FaIR can be run in large ensembles, accounting for key uncertainties.

In what follows, we use the AR6-tuned FaIR ensemble to compute the distribution of ZEC/T_{ze} consistent with the key findings of the AR6 report[32]. This ensemble consists of roughly 10^3 members, constrained out of a 10^6-member prior ensemble to replicate AR6-assessed ranges of climate metrics (including ECS, TCR, and radiative forcing) and selected to match historical observations of global-mean temperature, ocean heat uptake, and CO_2 concentrations (see Methods). This ensemble, therefore, provides a joint inference of the four

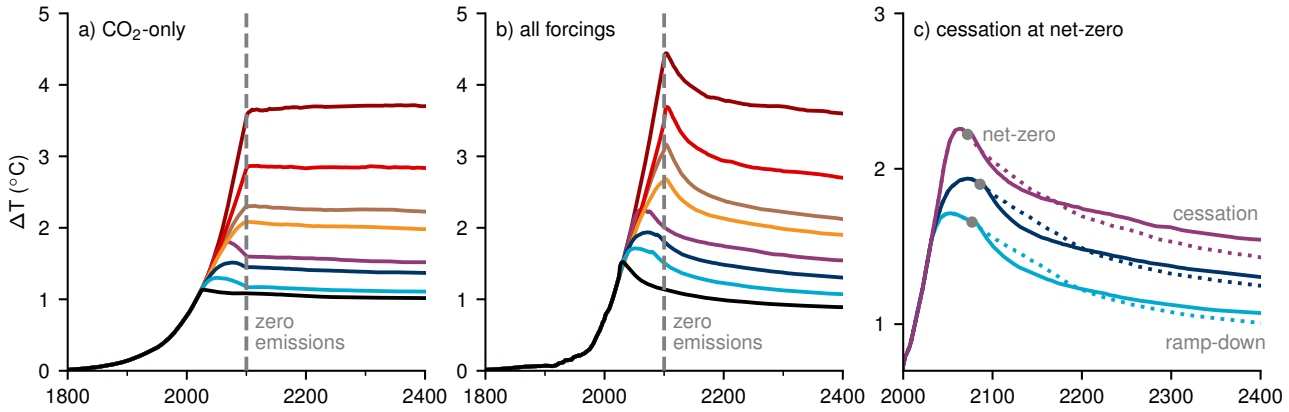

Fig. 3 Emissions cessation experiments reveal cooling after net zero. The median temperature response to emissions cessation in the Shared Socioeconomic Pathways (SSPs) given only CO_2 emissions (a) and all forcings (b+c) as projected by the FaIR ensemble. The scenarios in descending order are SSP5-8.5, SSP3-7.0, SSP2-4.5, SSP5-3.4, SSP4-3.4, SSP1-2.6, SSP1-1.9, and historical (black). In panels a and b, cessation occurs in 2100, whereas in panel c, at the time of net-zero greenhouse gas emissions (circles), emissions immediately cease (solid) or ramp-down (dotted) over the subsequent century.

parameters needed to evaluate ZEC, which captures the covariances implied by multiple lines of evidence (see Supplemental Figure 2).

Driving the ensemble with historical emissions followed by cessation at present yields the experimental ZEC/T_{ze} probability density function (PDF) shown in Figure 2(b), indicating that given our best estimates and associated uncertainties, there is a greater than 90% chance that emissions cessation today stops temperature rise, even on multi-century timescales. As evidenced by the scatter points in Figure 2(b), evaluating the analytic formula with each member's forcing and thermal disequilibrium yields essentially the same result.

Closer agreement between Eqn. 4 and FaIR, compared to with ZECMIP models, is unsurprising. Many of the full-complexity models suffer from energy imbalance at the start of the ZECMIP simulations (Supplemental Figure 7). In addition, the ECS values in FaIR correspond to true equilibrium values, while in full-complexity models, ECS is extrapolated from transient runs, making the ECS values inputted into the formula another possible source of error for more complex models. Finally, FaIR is a box model with well-separated fast and slow modes, matching the structural assumptions underlying the formula, while ZECMIP models exhibit greater structural complexity. Nonetheless, Fig. 2a suggests that most of the spread in normalized ZEC across the ZECMIP models is parametric and captured by uncertainty in two quantities: TCR/ECS and F_f/F_{ze}.

Central estimates of these parameters indicate significant cooling when all forcings are considered, but only minor cooling when CO_2 is the sole forcing. Evaluating the analytic formula with only the CO_2 component of present-day forcing–estimated at 2.3 W/m^2 [28]–yields $ZEC/T_{ze} = -0.1$. As demonstrated by the black curve in Figure 3a, the FaIR ensemble driven by only historical CO_2 emissions with emissions cessation at present day yields a relatively flat temperature response. The ensemble's estimate for CO_2-only historical ZEC is -0.1 [-0.3 to 0.2], with a 75% probability of cooling for CO_2-only historical ZEC (Supplemental Figure 9), consistent with the majority of ZECMIP CO_2-only results in Figure 2a.

Adding in the mostly short-lived non-CO_2 species yields more negative ZEC values, as demonstrated by the black curve in Figure 3b. Here FaIR is driven with all forcings up to emissions cessation at present day (2024). The additional forcing elevates F_{ze} above the CO_2-only value, but does not significantly raise F_f, given the shorter-lived nature of non-CO_2 species. Therefore, cooling in the all forcings case arises from combining transient non-CO_2 warming with a relatively flat temperature response to only CO_2.

This finding generalizes to the Shared Socieconomic Pathways (SSPs) as demonstrated by the colored lines in Figure 3a,b. Here the AR6-tuned FaIR ensemble is driven by each emissions pathway up to 2100, after which all emissions are zeroed. CO_2-only SSP experiments are shown in Figure 3a, and again exhibit relatively little change after cessation. Repeating these experiments with all forcings yields substantial cooling after emissions cessation (Figure 3b). As detailed in Supplementary Figure 11, the FaIR ensemble estimates a 89% or greater probability that long-term ZEC is negative in the SSPs. Cooling in the SSPs again results from decaying non-CO_2 warming superimposed on a relatively flat CO_2-only response.

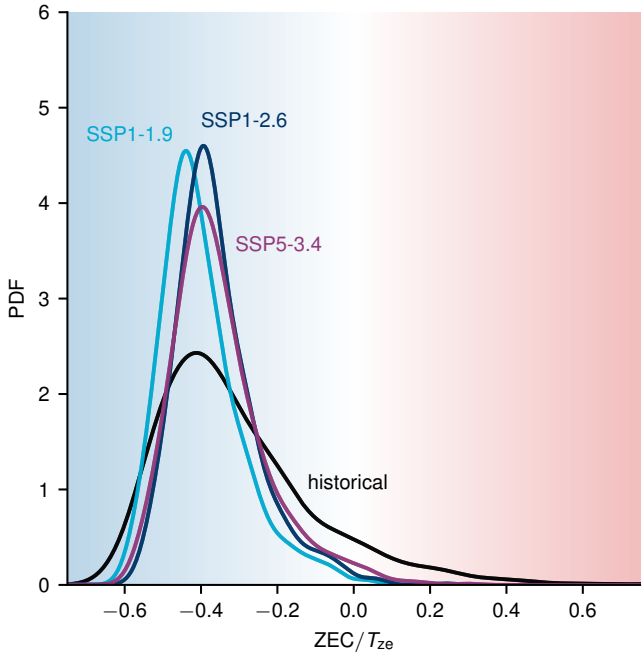

Fig. 4 Cooling distributions. Probability density functions (PDFs) of the fractional change in temperature after net-zero in the relevant SSPs (colors) and given no future emissions (black) as realized by the FaIR ensemble. PDFs are kernel density estimates with bandwidths set by Silverman's rule [27].

Cooling after net zero in the SSPs

We now shift our attention from climate change after emissions cessation to climate change after net-zero greenhouse gas emissions (hereafter, net-zero). Net-zero emissions result from offsetting positive emissions of minor GHGs with negative CO_2 emissions. Here we define net-zero with respect to the total global warming potential over 100 years (GWP100) assessed in AR6 [37].

As claimed earlier, the temperature responses to net-zero and zero emissions are closely related. In Figure 3c, we compare emissions cessation at net-zero (solid curve) to maintaining net-zero emissions (dotted curve) with offsetting emissions. Offsetting, however, cannot continue indefinitely, due to the finite capacities of negative emissions technologies and land-use strategies [38]. To extend the SSPs beyond the time of net-zero, the dotted curves in Figure 3c assume a linear ramp-down of net-zero emissions levels over the subsequent century. (The standard SSP extensions result in net negative emissions, and are thus not explored here.)

The relationship between the ramp-down and immediate cessation experiments can be understood as follows. By design, active net-zero emissions yield temperatures comparable to zero emissions over the near term. However, in the long-term, continued offsetting of minor GHG emissions with negative CO_2 emissions yields a lower long-term forcing in the net-zero case, as CO_2 is the longest-lived GHG. In this manner, the long-term temperature that results from ceasing emissions at net-zero provides a general upper bound on the long-term temperature that evolves under active net-zero GHG emissions.

Cessation experiments in Figure 3c provide a median estimate of this upper bound, indicating at least a 38% cooling following net-zero emissions in scenarios where offset emissions persist. Median estimates are similar across scenarios, due to limited changes in F_f/F_{ze} and $T/\tilde{T}$ between the present and the time of net-zero emissions (indicated by the circle in Fig. 3b). To the extent that the ocean thermodynamics and carbon cycle do advance toward equilibrium between today and net-zero, these effects largely compensate, leaving ZEC/T_{ze} roughly fixed (Supplemental Figure 6).

Figure 4 explores the uncertainty in these upper bounds by comparing the ZEC/T_{ze} distributions to the historical case. While all share similar median estimates, cooling is more likely in the SSPs. The narrower probability density functions (PDFs) for the SSPs are linked to greater confidence in the aerosol forcing at net-zero compared to present-day. Aerosol forcing is presently $-1.2\,[-2.1\,\text{to}\,-0.5]\,\text{W/m}^2$ [28], but contributes only $-0.14\,[-0.27\,\text{to}\,0.01]\,\text{W/m}^2$ at net-zero in SSP1-1.9, for instance. Lower aerosol forcing narrows the spread in F_{ze} and thus ZEC/T_{ze} (and eliminates the temperature spike exhibited by the historical curve in Figure 3b). Given this reduced uncertainty, cooling after net-zero is *extremely likely* ($> 95\%$ probability) in the FaIR ensemble. The balance of evidence, therefore, strongly indicates that the decrease in radiative heating (due to natural sinks) overcomes the loss of the ocean heat sink, yielding cooling after net-zero.

These findings contextualize two recent studies of FaIR's multi-*decadal* response to zero and net-zero emissions [39, 40]. After net-zero was reached in 2050 following a 1.5°C stabilization pathway, ref. [39] found a likely temperature decline of −0.1°C over the subsequent decades. Ref. [40] simulated FaIR's temperature response to present-day cessation through the end of the century, yielding results consistent with the 21st-century segment of the historical ZEC simulation presented here (black curve, Figure 3b). The present study demonstrates how these multi-decadal findings fit into a larger multi-century decline, which generalizes across the SSPs, emerges from the interplay between an enduring CO_2 response and transient non-CO_2 heating, and is predicted by key climate metrics via a simple formula (Eqn. 4).

Caveats

The magnitude of cooling after net-zero is additionally sensitive to the fate of managed lands. In Fig. 3b, we did not restore managed lands to their preindustrial state. Rather, we fixed the land-use albedo forcing ($-0.2\,\mathrm{W/m^2}$) and left the carbon sink unmodified. (Note that negative land-use albedo forcing yields the slightly lower long-term values in Fig. 3b compared to Fig. 3a.) However, if we cease land use altogether, ecosystems recover, modifying the albedo and taking up additional carbon. We crudely represent this in additional FaIR experiments by allowing ecosystem restoration to draw down historical land-use emissions ($\approx$ 250 GtC) on a centennial timescale [41]. As illustrated in Supplemental Figure 3, ecosystem restoration lowers ZEC/T_{ze} from roughly −30% to −50%.

Our analysis does not include permafrost processes, which remain uncertain and are omitted from most CMIP6 projections. Reversing the roughly −0.5° C cooling trends in Figure 3c would require a substantial net carbon loss from permafrost regions—on the order of 300 GtC, based on the AR6 central assessment of 1.65° C warming per 1000 GtC of CO_2 emissions [42]. However, a recent comparison [43] of models that do include permafrost processes found a net carbon *gain* of 8–244 GtC in these regions under a middle-of-the-road emissions scenario (RCP4.5 extended to 2300), as increased vegetation growth outweighed thaw-induced decomposition. Therefore, incorporating permafrost processes seems unlikely to overturn our main conclusions.

The ZEC formula indicates eventual cooling after net-zero, but the formula cannot rule out a transient peak. After net-zero, FaIR indeed monotonically cools to lower equilibrium temperatures, but FaIR's reduced complexity could be limiting its ability to resolve a transient peak. Such a transient peak in the all-forcings ZEC would have to emerge from a strong peak in the CO_2-only ZEC response overcoming cooling from declining shorter-lived forcings. Of the greater complexity models participating in ZECMIP, IAPRAS is the only model that demonstrates a CO_2-only response with a post-warming peak of sufficient magnitude (≈ 0.4°C) to plausibly imprint itself on the all-forcings case (Supplemental Figure 5a); however, IAPRAS also suffers from an anomalous and perplexing reversal in the sign of the top-of-atmosphere energy flux at emissions cessation, raising concerns over the physicality of this result (Supplemental Figure 5b).

While the evidence points to net-zero likely halting warming across timescales, we note that stopping temperature rise does not reverse the intensifying trend of many climate-change impacts. Even at fixed temperature, the continued oceanic uptake of heat and carbon is expected to raise sea levels and acidify the ocean [4, 44].

Conclusions

Our findings alleviate concerns raised in AR6 (and prompted by CO_2-only ZECMIP experiments) that the climate may continue to slowly warm after net-zero emissions. By linking the Zero Emissions Commitment (ZEC) response to established climate metrics through an analytic formula, we show that a strongly positive CO_2-only ZEC is unlikely. Moreover, when non–CO_2 forcings are included, the ZEC response shifts decisively toward cooling. Finally, we find that the ZEC represents an upper bound on the actual long-term temperatures after net zero. Collectively, these insights strongly suggest gradual cooling after net zero.

Methods

Fast and slow modes of warming

The two-box model provides a conceptual framework for understanding transient warming in climate models [17–19, 45]. The lower box represents the deep ocean, and the upper box combines the ocean's mixed layer and the atmosphere. The energy budget of the surface and deep-ocean box, respectively, are approximated as

$$C_{\mathrm{s}}\frac{dT}{dt} = F - \lambda T - \lambda'(T - T_d) - \gamma(T - T_{\mathrm{d}})\,, \tag{5}$$

$$C_{\mathrm{d}} \frac{dT_{\mathrm{d}}}{dt} = \gamma (T - T_{\mathrm{d}}) \,, \tag{6}$$

where T and T_{d} are the temperature anomalies (rel. preindustrial) of the respective boxes; C_{s} is the surface ocean's heat capacity (per area with units of $\mathrm{J/K/m^2}$); F is the radiative forcing (units of $\mathrm{W/m^2}$); γ is the heat transfer coefficient between the two ocean layers (units of $\mathrm{W/m^2/K}$); and λ is the equilibrium feedback parameter, i.e., the change in the top-of-atmosphere outgoing radiation per change in surface temperature at equilibrium (in units of $\mathrm{W/m^2/K}$). Finally, λ' represents the transient deviation in the feedback parameter (a.k.a., the pattern effect), driven primarily by cloud and ice-albedo dynamics that evolve with warming [e.g., 19, 46, 47].

When fit to full-complexity simulations, the response of the two-box model can be decomposed into a fast mode that responds to forcing in approximately five years, and a slow mode that warms over a few centuries [17, 18, 20, 48]. The fast mode is characterized by a negligible deep-ocean response ($T_d \to 0$) and surface quasi-equilibrium ($C_{\mathrm{s}}\, dT/dt \to 0$):

$$T_{\mathrm{fast}} \approx \frac{F}{\lambda + \lambda' + \gamma} \,. \tag{7}$$

The magnitude of the fast mode can be calibrated against the standard 1%/yr increase in CO_2 experiment. In year 70, the forcing corresponds to a CO_2 doubling, $F_{2\times}$, and the temperature anomaly is defined as the transient climate response: $\mathrm{TCR} \approx F_{2\times}/(\lambda + \lambda' + \gamma)$. Substituting this result into Eqn. 7 yields a general approximation for the fast-mode response:

$$T_{\mathrm{fast}} \approx \mathrm{TCR} \left(\frac{F}{F_{2\times}} \right) \,, \tag{8}$$

which accurately replicates historical temperatures (Supplemental Figure 8).

Define $\tilde{T}$ to be the equilibrium warming expected if F were held fixed: $\tilde{T} = F/\lambda$. By the definition of the equilibrium climate sensitivity (ECS), note that $\lambda = F_{2\times}/\mathrm{ECS}$ and thus $\tilde{T} = \mathrm{ECS}\,(F/F_{2\times})$. Therefore, in the only-fast-mode regime, the thermal disequilibrium is given by,

$$\frac{T_{\mathrm{fast}}}{\tilde{T}} = \frac{\mathrm{TCR}}{\mathrm{ECS}} \,. \tag{9}$$

In the net-zero scenarios, $T/\tilde{T}$ increases over time due to the gradually evolving slow mode; the largest effect occurs for SSP1-1.9, in which the surface temperature stabilizes, affording the deep-ocean the opportunity to raise $T/\tilde{T}$ from near 0.6 at present to 0.8 by the end of the century (Supplementary Figure 6a).

Note that the analytical formula (and the FaIR climate model) assumes that warming is paced by approximately two modes that are well seperated in time. The finding that a 1D diffusive model (which possesses modes at all timescales) provides equivalently accurate fits to comprehensive models [49] poses a challenge to this framework. Because historical forcing has increased slower than the 1%/yr trajectory, a diffusive model would suggest that we are closer to thermal equilibrium with our current forcing than the 1%/yr-driven ocean is with $F_{2\times}$ at the time of doubling (year 70). Therefore, in a diffusive model, present-day $T/\tilde{T}$ would be greater than TCR/ECS, implying even greater cooling after zero emissions: the closer the ocean is to thermal equilibrium with present-day forcing, the more the decline in forcing dominates the zero-emissions response. Replacing the two-box model with a 1D diffusive model would therefore strengthen, rather than contradict, our main findings.

Final forcing

CO_2 is the dominant forcing on multi-century timescales (Supplementary Figure 13). Radiative forcing from CO_2 is approximately logarithmic in the concentration, or equivalently, in the mass of airborne CO_2 [50]:

$$F_{\mathrm{CO_2}}(t) \approx F_o \log\left(1 + A(t)\, C_{\mathrm{emit}}(t)/C_{\mathrm{pre}}\right) \,, \tag{10}$$

where $C_{\mathrm{pre}} \approx 590\,\mathrm{GtC}$ is the pre-industrial mass of atmospheric carbon, $A(t)$ is the airborne fraction of cumulative emissions C_{emit} (currently 740 GtC), and $F_o \approx 5.6\,\mathrm{W/m^2}$ [28, 41].

Carbon-cycle projections find that roughly 20% of cumulative emissions are stranded in the atmosphere on multi-century timescales [10, 31, 51], in agreement with carbon-chemistry theory [52]. Evaluating eqn. 10 with a final airborne fraction of $A_{\mathrm{f}} \approx 0.2$ yields a final CO_2 forcing of $1.2\,\mathrm{W/m^2}$, close to the central value found in FaIR ($1.3\,\mathrm{W/m^2}$).

The total forcing in the primary FaIR experiments (Fig. 3b) additionally includes $-0.2\,\mathrm{W/m^2}$ of albedo change from land use, yielding $F_\mathrm{f} = 1.1\,\mathrm{W/m^2}$. If land-use ceases altogether, biomass recovers, reducing the albedo forcing. Restoring biomass also lowers the CO_2 forcing by drawing down prior land-use emissions. In an alternate experiment (Supplemental Figure 3), restoring biomass on managed land to preindustrial values yields an additional 0.2 °C of eventual cooling.

Finally, we consider the sensitivity of our findings to uncertainty in A_f. If we recompute the final temperature with A_f sampled from the ZECMIP ensemble instead of FaIR, the resultant $\mathrm{ZEC}/T_\mathrm{ze}$ distribution shifts towards greater cooling (Supplemental Figure 11), due to a lower median A_f in ZECMIP..

CO_2-only case

If CO_2 is the only forcing (as in Figure 3a), the forcing disequilibrium can be directly related to the disequilibrium in the carbon system. Given the airborne fractions A_ze and A_f in the zero-emissions state and final state, respectively, Eqn. 10 yields

$$\frac{F_\mathrm{f}}{F_\mathrm{ze}} = \frac{\log\left(1 + A_\mathrm{f}\, C_\mathrm{emit}/C_\mathrm{pre}\right)}{\log\left(1 + A_\mathrm{ze} C_\mathrm{emit}/C_\mathrm{pre}\right)} \approx \frac{A_\mathrm{f}}{A_\mathrm{ze}}\,, \tag{11}$$

where we linearized by assuming $C_\mathrm{emit} \ll C_\mathrm{pre}/A_\mathrm{ze} \approx 1500$ GtC, estimated given the present-day airborne fraction (≈ 0.5; [41]). The post-emissions response is then determined by simply comparing the *carbon* disequilibrium ($A_\mathrm{f}/A_\mathrm{ze}$) to the thermal disequilibrium:

$$\frac{\mathrm{ZEC}}{T_{ze}} \approx \frac{A_\mathrm{f}/A_\mathrm{ze}}{\mathrm{TCR/ECS}} - 1\,. \tag{12}$$

The nearly flat responses in Figure 3a arise because the carbon and thermal disequilibria are both about 1/2, which, according to the formula above, yields a CO_2-only ZEC of approximately zero.

ZECMIP

To account for natural variability, the zero-emissions temperature T_ze is taken to be the 20-year average centered on the time of zero emissions. The final temperature T_f is the average over the last 20 years in each simulation. The majority of ZECMIP simulations are of too-short duration to reach the final carbon and thermal equilibria. If the simulated final state is out of thermal equilibrium, planetary energy balance yields $\epsilon N_\mathrm{f} = F_\mathrm{f} - \lambda T_\mathrm{f}$, where N_f is the top of the atmosphere energy imbalance (units of $\mathrm{W/m^2}$), and here ϵ is the efficacy of planetary heat uptake. This serves as an alternative parameterization of the pattern effect (rather than λ' as in Eqn. 6), which we employ here because values of ϵ have been previously fit to the ZECMIP models [10]. We approximate ϵ as constant and use the value fit to years 10 through 140 of the 1%/yr CO_2 computed in ref. [10].

Repeating the derivation of the ZEC formula with $T_\mathrm{f} = (F_\mathrm{f} - \epsilon N_\mathrm{f})/\lambda$ yields

$$\frac{\mathrm{ZEC}}{T_{ze}} \approx \frac{(F_\mathrm{f} - \epsilon N_\mathrm{f})/F_\mathrm{ze}}{\mathrm{TCR/ECS}} - 1\,, \tag{13}$$

which is plotted in Figure 2. A subset of models have a non-zero N at the simulation's start due to energy conservation error or insufficient spin-up time. We compute N_f relative to this preindustrial imbalance, estimated as the y-intercept of a linear regression of N versus F over the first 20 years of data (Supplementary Figure 7).

FaIR

To understand how estimates of key climate metrics covary, and to project future temperatures in line with AR6 uncertainties, we rely on a reduced-complexity model ensemble. Reduced-complexity models can be run in larger ensembles and more effectively tuned to match target distributions than resource-intensive CMIP models [34]. Here we use the Finite Amplitude Impulse Response (FaIR) ensemble, arising from IPCC efforts to build a model ensemble consistent with their integrated assessments [32, 33, 35, 53]. We rely on the AR6-tuned FaIR ensemble, which is fully described in [35], and calibrated to AR6 in [32].

We briefly note that FaIR consists of a three-layer energy balance coupled to a basic carbon-cycle model. Carbon uptake is parameterized via a four-timescale impulse response function with state-dependent adjustments to incorporate carbon-climate feedbacks. Simple treatments of methane chemistry, aerosol direct and cloud-interaction effects, land-use albedo, and other minor GHGs are also included (see ref. [35] for details) and calibrated to match AR6 distributions [32]. For the historical ZEC experiment, we drive the FaIR ensemble with the latest Indicators of Global Climate Change (IGCC) emissions reconstruction [28]. Future projections

are driven with emissions from the Shared Socioeconomic Pathways [38]. In ZEC experiments, anthropogenic emissions are zeroed by instantaneously reverting all emissions to pre-industrial (1750) baselines.

Supplementary information. Supplementary Figures 1-13 are attatched to this manuscript.

Acknowledgements. N.T. is supported by the Kernan Brothers Environmental Fellowship at the Harvard University Center for the Environment.

Author contributions. N.T. and N.J. designed the research. N.T. derived the formalism, performed the analysis, and wrote the manuscript. All authors contributed to revising the manuscript.

Code and data availability

The code and data required to reproduce our findings are available in a Zenodo repository at https://doi.org/10.5281/zenodo.10120439.

References

[1] United Nations: Paris agreement. United Nations Treaty Series **Treaty No. XXVII-7-d** (2015)

[2] Matthews, H.D., Caldeira, K.: Stabilizing climate requires near-zero emissions. Geophysical Research Letters **35**(4) (2008) https://doi.org/10.1029/2007GL032388

[3] Allen, M.R., Frame, D.J., Huntingford, C., Jones, C.D., Lowe, J.A., Meinshausen, M., Meinshausen, N.: Warming caused by cumulative carbon emissions towards the trillionth tonne. Nature **458**(7242), 1163–1166 (2009)

[4] Solomon, S., Plattner, G.-K., Knutti, R., Friedlingstein, P.: Irreversible climate change due to carbon dioxide emissions. Proceedings of the national academy of sciences **106**(6), 1704–1709 (2009)

[5] United Nations Framework Convention on Climate Change, Article 2 (1992)

[6] Gillett, N.P., Arora, V.K., Zickfeld, K., Marshall, S.J., Merryfield, W.J.: Ongoing climate change following a complete cessation of carbon dioxide emissions. Nature Geoscience **4**(2), 83–87 (2011) https://doi.org/10.1038/ngeo1047

[7] Hare, B., Meinshausen, M.: How much warming are we committed to and how much can be avoided? Climatic Change **75**(1), 111–149 (2006)

[8] Zickfeld, K., Eby, M., Weaver, A.J., Alexander, K., Crespin, E., Edwards, N.R., Eliseev, A.V., Feulner, G., Fichefet, T., Forest, C.E., Friedlingstein, P., Goosse, H., Holden, P.B., Joos, F., Kawamiya, M., Kicklighter, D., Kienert, H., Matsumoto, K., Mokhov, I.I., Monier, E., Olsen, S.M., Pedersen, J.O.P., Perrette, M., Philippon-Berthier, G., Ridgwell, A., Schlosser, A., Von Deimling, T.S., Shaffer, G., Sokolov, A., Spahni, R., Steinacher, M., Tachiiri, K., Tokos, K.S., Yoshimori, M., Zeng, N., Zhao, F.: Long-Term climate change commitment and reversibility: An EMIC intercomparison. Journal of Climate **26**(16), 5782–5809 (2013) https://doi.org/10.1175/JCLI-D-12-00584.1

[9] Ehlert, D., Zickfeld, K.: What determines the warming commitment after cessation of CO2 emissions? Environmental Research Letters **12**(1), 015002 (2017)

[10] MacDougall, A.H., Frölicher, T.L., Jones, C.D., Rogelj, J., Matthews, H.D., Zickfeld, K., Arora, V.K., Barrett, N.J., Brovkin, V., Burger, F.A., Eby, M., Eliseev, A.V., Hajima, T., Holden, P.B., Jeltsch-Thömmes, A., Koven, C., Mengis, N., Menviel, L., Michou, M., Mokhov, I.I., Oka, A., Schwinger, J., Séférian, R., Shaffer, G., Sokolov, A., Tachiiri, K., Tjiputra, J., Wiltshire, A., Ziehn, T.: Is there warming in the pipeline? a multi-model analysis of the zero emissions commitment from co_2. Biogeosciences **17**(11), 2987–3016 (2020) https://doi.org/10.5194/bg-17-2987-2020

[11] Lee, J.Y., Marotzke, J., Bala, G., Cao, L., Corti, S., Dunne, J.P., Engelbrecht, F., Fischer, E., Fyfe, J.C., Jones, C., Maycock, A., Mutemi, J., Ndiaye, O., Panickal, S., Zhou, T.: Future Global Climate: Scenario-Based Projections and Near-Term Information. Cambridge University Press, Cambridge, United Kingdom and New York, NY, USA (2021)

[12] Rogelj, J., Shindell, D., Jiang, K., Fifita, S., Forster, P., Ginzburg, V., Handa, C., Kheshgi, H., Kobayashi, S., Kriegler, E., Mundaca, L., Séférian, R., Vilariño, M.V.: Mitigation Pathways Compatible with 1.5°C in the Context of Sustainable Development. In: Global Warming of 1.5°C: An IPCC Special Report on the Impacts of Global Warming of 1.5°C Above Pre-industrial Levels and Related Global Greenhouse Gas Emission Pathways, in the Context of Strengthening the Global Response to the Threat of Climate Change, Sustainable Development, and Efforts to Eradicate poverty. World Meteorological Organization, Geneva, Switzerland (2018)

[13] Palazzo Corner, S., al.: The zero emissions commitment and climate stabilization. Frontiers in Science **1** (2023) https://doi.org/10.3389/fsci.2023.1170744

[14] Matthews, H.D., Gillett, N.P., Stott, P.A., Zickfeld, K.: The proportionality of global warming to cumulative carbon emissions. Nature **459**(7248), 829–832 (2009)

[15] Rogelj, J., Forster, P.M., Kriegler, E., Smith, C.J., Séférian, R.: Estimating and tracking the remaining carbon budget for stringent climate targets. Nature **571**(7765), 335–342 (2019)

[16] Canadell, J.G., Monteiro, P.M.S., Costa, M.H., Cunha, L., Cox, P.M., Eliseev, A.V., Henson, S., Ishii, M., Jaccard, S., Koven, C., Lohila, A., Patra, P.K., Piao, S., Rogelj, J., Syampungani, S., Zaehle, S., Zickfeld, K.: Global carbon and other biogeochemical cycles and feedbacks. In: Climate Change 2021: The Physical Science Basis. Contribution of Working Group I to the Sixth Assessment Report of the Intergovernmental Panel on Climate Change. Cambridge University Press, Cambridge, UK and New York, NY, USA (2021). https://doi.org/10.1017/9781009157896.007

[17] Gregory, J.M.: Vertical heat transports in the ocean and their effect on time-dependent climate change. Climate Dynamics **16**(7), 501–515 (2000)

[18] Held, I.M., Winton, M., Takahashi, K., Delworth, T., Zeng, F., Vallis, G.K.: Probing the fast and slow components of global warming by returning abruptly to preindustrial forcing. Journal of Climate **23**(9), 2418–2427 (2010)

[19] Armour, K.C.: Energy budget constraints on climate sensitivity in light of inconstant climate feedbacks. Nature Climate Change **7**(5), 331–335 (2017)

[20] Geoffroy, O., Saint-Martin, D., Olivié, D.J.L., Voldoire, A., Bellon, G., Tytéca, S.: Transient climate response in a two-layer energy-balance model. part i: Analytical solution and parameter calibration using cmip5 aogcm experiments. Journal of Climate **26**(6), 1841–1857 (2013) https://doi.org/10.1175/JCLI-D-12-00195.1

[21] Covey, C., AchutaRao, K.M., Cubasch, U., Jones, P., Lambert, S.J., Mann, M.E., Phillips, T.J., Taylor, K.E.: An overview of results from the coupled model intercomparison project. Global and Planetary Change **37**(1), 103–133 (2003) https://doi.org/10.1016/S0921-8181(02)00193-5

[22] Eyring, V., Bony, S., Meehl, G.A., Senior, C.A., Stevens, B., Stouffer, R.J., Taylor, K.E.: Overview of the coupled model intercomparison project phase 6 (cmip6) experimental design and organization. Geoscientific Model Development **9**(5), 1937–1958 (2016) https://doi.org/10.5194/gmd-9-1937-2016

[23] Sherwood, S.C., Webb, M.J., Annan, J.D., Armour, K.C., Forster, P.M., Hargreaves, J.C., Hegerl, G., Klein, S.A., Marvel, K.D., Rohling, E.J., Watanabe, M., Andrews, T., Braconnot, P., Bretherton, C.S., Foster, G.L., Hausfather, Z., Heydt, A.S., Knutti, R., Mauritsen, T., Norris, J.R., Proistosescu, C., Rugenstein, M., Schmidt, G.A., Tokarska, K.B., Zelinka, M.D.: An assessment of earth's climate sensitivity using multiple lines of evidence. Reviews of Geophysics **58**(4) (2020) https://doi.org/10.1029/2019RG000678

[24] Climate Change, I.P.: Climate Change 2013 – The Physical Science Basis: Working Group I Contribution to the Fifth Assessment Report of the Intergovernmental Panel on Climate Change. Cambridge University Press, ??? (2014). https://doi.org/10.1017/CBO9781107415324

[25] Williams, R.G., Roussenov, V., Frölicher, T.L., Goodwin, P.: Drivers of continued surface warming after cessation of carbon emissions. Geophysical Research Letters **44**(20), 10633–10642 (2017) https://doi.org/10.1002/2017GL075080

[26] Allen, M.R., Friedlingstein, P., Girardin, C.A., Jenkins, S., Malhi, Y., Mitchell-Larson, E., Peters, G.P., Rajamani, L.: Net zero: science, origins, and implications. Annual Review of Environment and Resources **47**, 849–887 (2022)

[27] Silverman, B.W.: Density Estimation for Statistics and Data Analysis, p. 45. Chapman & Hall/CRC, London (1986)

[28] Forster, P.M., Smith, C., Walsh, T., Lamb, W.F., Lamboll, R., Hall, B., Hauser, M., Ribes, A., Rosen, D., Gillett, N.P., Palmer, M.D., Rogelj, J., Schuckmann, K., Trewin, B., Allen, M., Andrew, R., Betts, R.A., Borger, A., Boyer, T., Broersma, J.A., Buontempo, C., Burgess, S., Cagnazzo, C., Cheng, L., Friedlingstein, P., Gettelman, A., Gütschow, J., Ishii, M., Jenkins, S., Lan, X., Morice, C., Mühle, J., Kadow, C., Kennedy, J., Killick, R.E., Krummel, P.B., Minx, J.C., Myhre, G., Naik, V., Peters, G.P., Pirani, A., Pongratz, J., Schleussner, C.-F., Seneviratne, S.I., Szopa, S., Thorne, P., Kovilakam, M.V.M., Majamäki, E., Jalkanen, J.-P., Marle, M., Hoesly, R.M., Rohde, R., Schumacher, D., Werf, G., Vose, R., Zickfeld, K., Zhang, X., Masson-Delmotte, V., Zhai, P.: Indicators of Global Climate Change 2023: annual update of key indicators of the state of the climate system and human influence. Earth System Science Data **16**(6), 2625–2658 (2024) https://doi.org/10.5194/essd-16-2625-2024

[29] Winton, M., Adcroft, A., Dunne, J.P., Held, I.M., Shevliakova, E., Zhao, M., Guo, H., Hurlin, W., Krasting, J., Knutson, T., Paynter, D., Silvers, L.G., Zhang, R.: Climate sensitivity of gfdl's cm4.0. Journal of Advances in Modeling Earth Systems **12**(1), 2019–001838 (2020) https://doi.org/10.1029/2019MS001838

[30] Forster, P., Storelvmo, T., Armour, K., Collins, W., Dufresne, J.L., Frame, D., Lunt, D.J., Mauritsen, T., Palmer, M.D., Watanabe, M., Wild, M., Zhang, H.: The earth's energy budget, climate feedbacks, and climate sensitivity. In: Climate Change 2021: The Physical Science Basis. Contribution of Working Group I to the Sixth Assessment Report of the Intergovernmental Panel on Climate Change. Cambridge University Press, Cambridge, United Kingdom and New York, NY, USA (2021)

[31] Archer, D., Eby, M., Brovkin, V., Ridgwell, A., Cao, L., Mikolajewicz, U., Caldeira, K., Matsumoto, K., Munhoven, G., Montenegro, A., *et al.*: Atmospheric lifetime of fossil fuel carbon dioxide. Annual review of earth and planetary sciences **37**, 117–134 (2009)

[32] Smith, C., Cummins, D.P., Fredriksen, H.-B., Nicholls, Z., Meinshausen, M., Allen, M., Jenkins, S., Leach, N., Mathison, C., Partanen, A.-I.: fair-calibrate v1.4.1: calibration, constraining and validation of the FaIR simple climate model for reliable future climate projections. EGUsphere **2024**, 1–36 (2024) https://doi.org/10.5194/egusphere-2024-708

[33] Smith, C.J., Forster, P.M., Allen, M., Leach, N., Millar, R.J., Passerello, G.A., Regayre, L.A.: FAIR v1.3: a simple emissions-based impulse response and carbon cycle model. Geoscientific Model Development **11**, 2273–2297 (2018) https://doi.org/10.5194/gmd-11-2273-2018

[34] Nicholls, Z.R.J., Meinshausen, M., Lewis, J., Gieseke, R., Dommenget, D., Dorheim, K., al.: Reduced complexity model intercomparison project phase 1: Introduction and evaluation of global-mean temperature response. Geoscientific Model Development **13**(11), 5175–5190 (2020) https://doi.org/10.5194/gmd-13-5175-2020

[35] Leach, N.J., Jenkins, S., Nicholls, Z., Smith, C.J., Lynch, J., Cain, M., Walsh, T., Wu, B., Tsutsui, J., Allen, M.R.: Fairv2. 0.0: a generalized impulse response model for climate uncertainty and future scenario exploration. Geoscientific Model Development **14**(5), 3007–3036 (2021)

[36] IPCC: Scenarios and modelling methods. In: Guivarch, C., Kriegler, E., Portugal-Pereira, J., Bosetti, V., Edmonds, J., Fischedick, M., Havlík, P., Jaramillo, P., Krey, V., Lecocq, F., Lucena, A., Meinshausen, M., Mirasgedis, S., O'Neill, B., Peters, G.P., Rogelj, J., Rose, S., Saheb, Y., Strbac, G., Hammer Strømman, A., Vuuren, D.P., Zhou, N. (eds.) Climate Change 2022: Mitigation of Climate Change. Contribution of Working Group III to the Sixth Assessment Report of the Intergovernmental Panel on Climate Change. Cambridge University Press, Cambridge, UK and New York, NY, USA (2022). Chap. Annex III. https://doi.org/10.1017/9781009157926.022

[37] Smith, C., Nicholls, Z.R.J., Armour, K., Collins, W., Forster, P., Meinshausen, M., Palmer, M.D., Watanabe, M.: The Earth's Energy Budget, Climate Feedbacks, and Climate Sensitivity Supplementary Material. In Climate Change 2021: The Physical Science Basis. Contribution of Working Group I to the Sixth Assessment Report of the Intergovernmental Panel on Climate Change (2021)

[38] Meinshausen, M., Nicholls, Z.R., Lewis, J., Gidden, M.J., Vogel, E., Freund, M., Beyerle, U., Gessner, C., Nauels, A., Bauer, N., *et al.*: The shared socio-economic pathway (ssp) greenhouse gas concentrations and their extensions to 2500. Geoscientific Model Development **13**(8), 3571–3605 (2020)

[39] Jenkins, S., Sanderson, B., Peters, G., Frölicher, T.L., Friedlingstein, P., Allen, M.: The multi-decadal response to net zero co2 emissions and implications for emissions policy. Geophysical Research Letters **49**, 2022–101047 (2022)

[40] Dvorak, M., Armour, K., Frierson, D., Proistosescu, C., Baker, M., Smith, C.: Estimating the timing of geophysical commitment to 1.5 and 2.0° c of global warming. Nature Climate Change **12**(6), 547–552 (2022)

[41] Friedlingstein, P., O'Sullivan, M., Jones, M.W., Andrew, R.M., Gregor, L., Hauck, J., Le Quéré, C., Luijkx, I.T., Olsen, A., Peters, G.P., Peters, W., Pongratz, J., Schwingshackl, C., Sitch, S., Canadell, J.G., Ciais, P., Jackson, R.B., Alin, S.R., Alkama, R., Arneth, A., Arora, V.K., Bates, N.R., Becker, M., Bellouin, N., Bittig, H.C., Bopp, L., Chevallier, F., Chini, L.P., Cronin, M., Evans, W., Falk, S., Feely, R.A., Gasser, T., Gehlen, M., Gkritzalis, T., Gloege, L., Grassi, G., Gruber, N., Gürses, O., Harris, I., Hefner, M., Houghton, R.A., Hurtt, G.C., Iida, Y., Ilyina, T., Jain, A.K., Jersild, A., Kadono, K., Kato, E., Kennedy, D., Klein Goldewijk, K., Knauer, J., Korsbakken, J.I., Landschützer, P., Lefèvre, N., Lindsay, K., Liu, J., Liu, Z., Marland, G., Mayot, N., McGrath, M.J., Metzl, N., Monacci, N.M., Munro, D.R., Nakaoka, S.-I., Niwa, Y., O'Brien, K., Ono, T., Palmer, P.I., Pan, N., Pierrot, D., Pocock, K., Poulter, B., Resplandy, L., Robertson, E., Rödenbeck, C., Rodriguez, C., Rosan, T.M., Schwinger, J., Séférian, R., Shutler, J.D., Skjelvan, I., Steinhoff, T., Sun, Q., Sutton, A.J., Sweeney, C., Takao, S., Tanhua, T., Tans, P.P., Tian, X., Tian, H., Tilbrook, B., Tsujino, H., Tubiello, F., Werf, G.R., Walker, A.P., Wanninkhof, R., Whitehead, C., Willstrand Wranne, A., Wright, R., Yuan, W., Yue, C., Yue, X., Zaehle, S., Zeng, J., Zheng, B.: Global carbon budget 2022. Earth System Science Data **14**(11), 4811–4900 (2022) https://doi.org/10.5194/essd-14-4811-2022

[42] Canadell, J.G., Monteiro, P.M.S., Costa, M.H., Cunha, L., Cox, P.M., Eliseev, A.V., Henson, S., Ishii, M., Jaccard, S., Koven, C., Lohila, A., Patra, P.K., Piao, S., Rogelj, J., Syampungani, S., Zaehle, S., Zickfeld, K.: Global carbon and other biogeochemical cycles and feedbacks. In: Climate Change 2021: The Physical Science Basis. Contribution of Working Group I to the Sixth Assessment Report of the Intergovernmental Panel on Climate Change. Cambridge University Press, Cambridge, UK and New York, NY, USA (2021). https://doi.org/10.1017/9781009157896.007

[43] McGuire, A.D., Lawrence, D.M., Koven, C., Clein, J.S., Burke, E., Chen, G., Jafarov, E., MacDougall, A.H., Marchenko, S., Nicolsky, D., *et al.*: Dependence of the evolution of carbon dynamics in the northern permafrost region on the trajectory of climate change. Proceedings of the National Academy of Sciences **115**(15), 3882–3887 (2018)

[44] IPCC: Summary for policymakers. In: Climate Change 2021: The Physical Science Basis. Contribution of Working Group I to the Sixth Assessment Report of the Intergovernmental Panel on Climate Change. Cambridge University Press, Cambridge, UK and New York, NY, USA (2021). https://doi.org/10.1017/9781009157896.001

[45] Jeevanjee, N.: The physics of climate change: simple models in climate science. arXiv (2018). https://doi.org/10.48550/ARXIV.1802.02695

[46] Rose, B.E., Armour, K.C., Battisti, D.S., Feldl, N., Koll, D.D.: The dependence of transient climate sensitivity and radiative feedbacks on the spatial pattern of ocean heat uptake. Geophysical Research Letters **41**(3), 1071–1078 (2014)

[47] Andrews, T., Bodas-Salcedo, A., Gregory, J.M., Dong, Y., Armour, K.C., Paynter, D., Lin, P., Modak, A., Mauritsen, T., Cole, J.N., *et al.*: On the effect of historical sst patterns on radiative feedback. Journal

of Geophysical Research: Atmospheres **127**(18), 2022–036675 (2022)

[48] Olivié, D.J.L., Peters, G.P., Saint-Martin, D.: Atmosphere response time scales estimated from aogcm experiments. Journal of Climate **25**(22), 7956–7972 (2012) https://doi.org/10.1175/JCLI-D-11-00475.1

[49] Caldeira, K., Myhrvold, N.P.: Projections of the pace of warming following an abrupt increase in atmospheric carbon dioxide concentration. Environmental Research Letters **8**(3), 034039 (2013) https://doi.org/10.1088/1748-9326/8/3/034039

[50] Pierrehumbert, R.T.: Principles of Planetary Climate. Cambridge University Press, ??? (2010)

[51] Eby, M., Zickfeld, K., Montenegro, A., Archer, D., Meissner, K., Weaver, A.: Lifetime of anthropogenic climate change: millennial time scales of potential co2 and surface temperature perturbations. Journal of climate **22**(10), 2501–2511 (2009)

[52] Goodwin, P., Williams, R.G., Follows, M.J., Dutkiewicz, S.: Ocean-atmosphere partitioning of anthropogenic carbon dioxide on centennial timescales. Global Biogeochemical Cycles **21**(1) (2007)

[53] Millar, R.J., Nicholls, Z.R., Friedlingstein, P., Allen, M.R.: A modified impulse-response representation of the global near-surface air temperature and atmospheric concentration response to carbon dioxide emissions. Atmospheric Chemistry and Physics **17**, 7213–7228 (2017) https://doi.org/10.5194/acp-17-7213-2017

Supplementary Figures

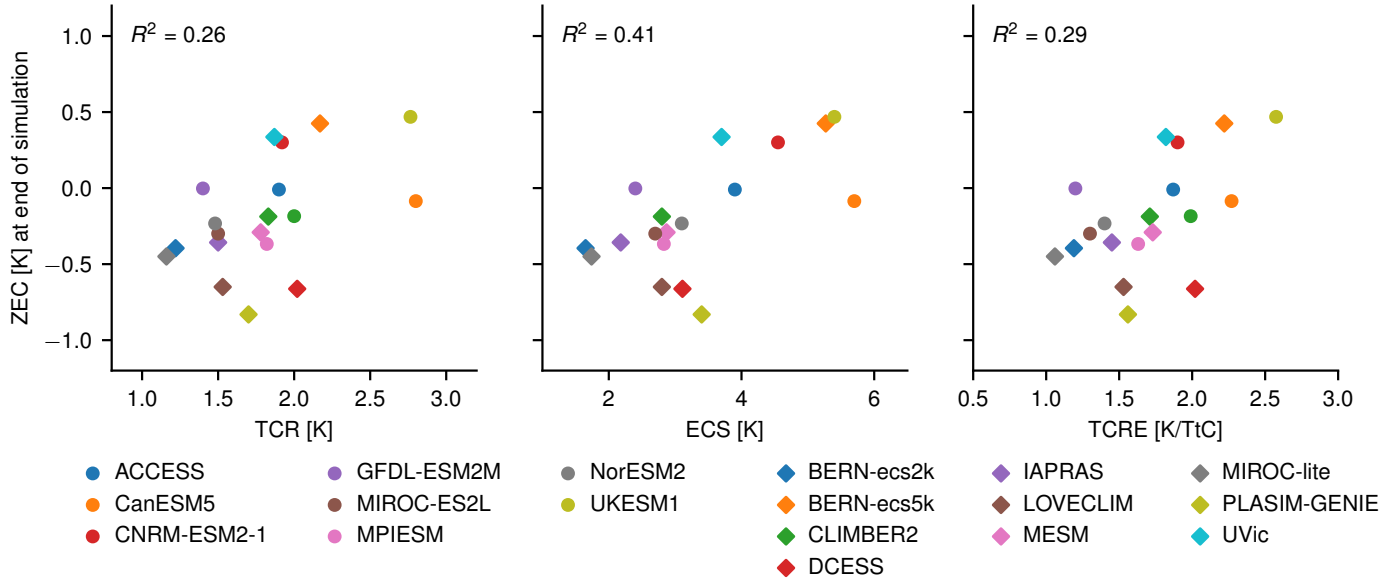

Supplementary Fig. 1 ZEC correlates weakly with established metrics. Correlations between ZEC realized in the ZECMIP 1000 GtC simulations (of varying duration) shown in Figure 1 of the main text and the transient climate response (left), equilibrium climate sensitivity (center), and the transient climate response to cumulative emissions (right).

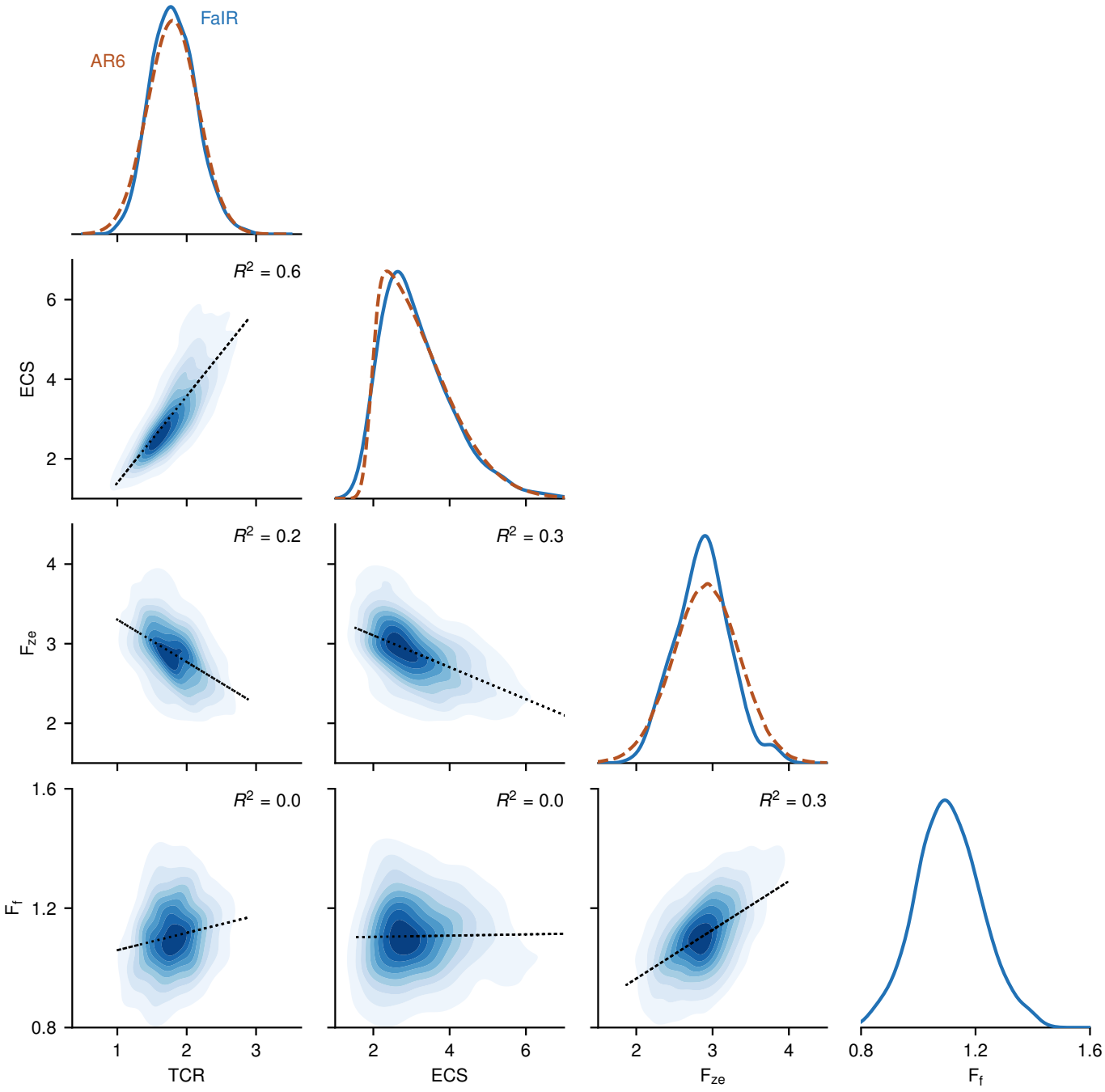

Supplementary Fig. 2 Estimates of distributions and covariances in the AR6-tuned FaIR ensemble. Diagonals present the kernel-density estimates of the 841-member ensemble of FaIR configurations, tuned to the AR6 report. See Methods for details. Off-diagonals show the kernel-density estimates for covariances betweeen the different variables that determine ZEC. The ensemble's TCR and ECS distribution are compared to the AR6 estimates. The present-day forcing, in this context, F_{ze}, is compared to the best estimate of 2023 forcing based on AR6 methods [28]. The final forcing after carbon equilibrium is not assessed in AR6, so no comparison is made.

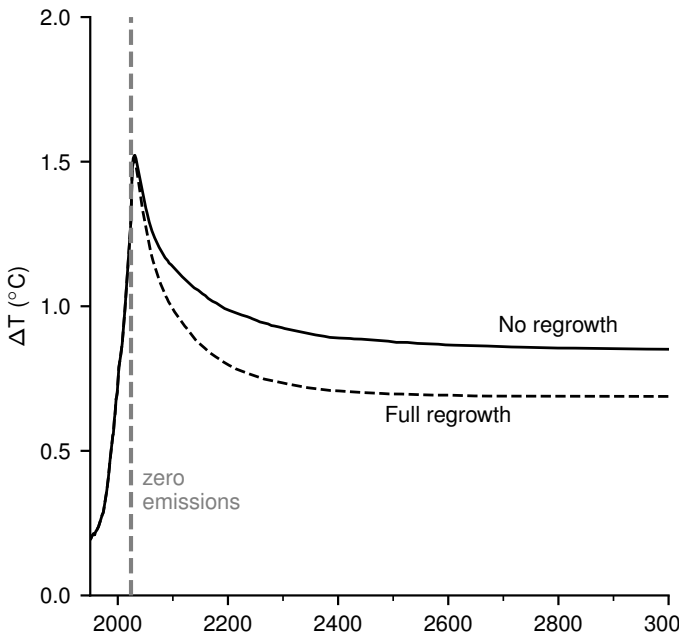

Supplementary Fig. 3 Including ecosystem restoration after emissions cessation. Median temperature response in the FaIR ensemble to immediate emissions cessation assuming no regrowth on managed land (solid) and full regrowth (dashed), modeled as reuptake of historical land-use emissions on a centennial *e*-folding timescale.

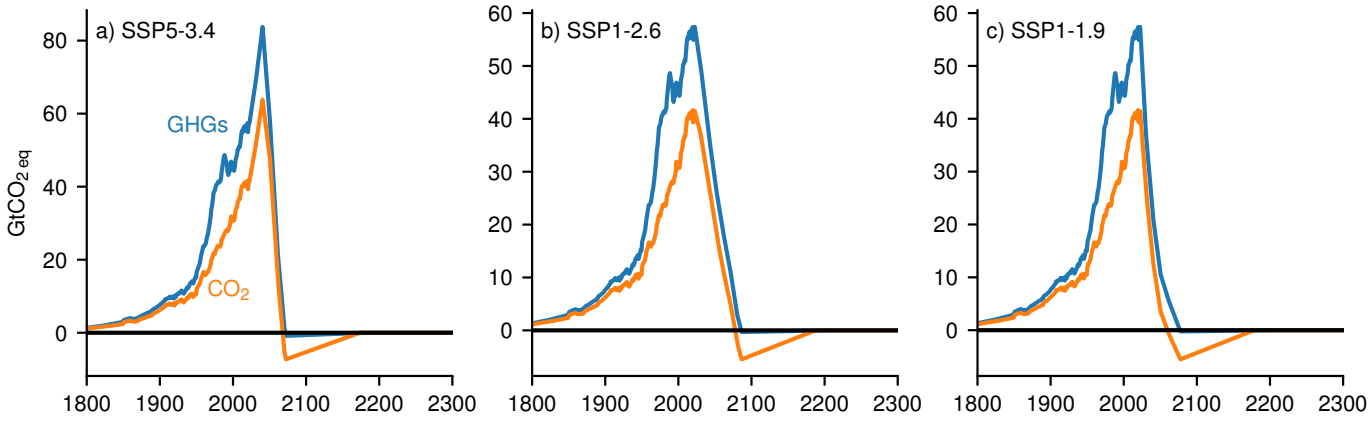

Supplementary Fig. 4 CO_2-equivalent emissions in the SSPs with ramp-down after net-zero. The Shared Socioeconomic Pathways (SSP) CO_2 and CO_2-eqiuvalent emissions for scenarios that achieve net-zero greenhouse gases this century [38], modified to linearly ramp-down emissions after net-zero. AR6 estimates of global warming potential at 100 years (GWP100) are used to compute CO_2-equivalent.

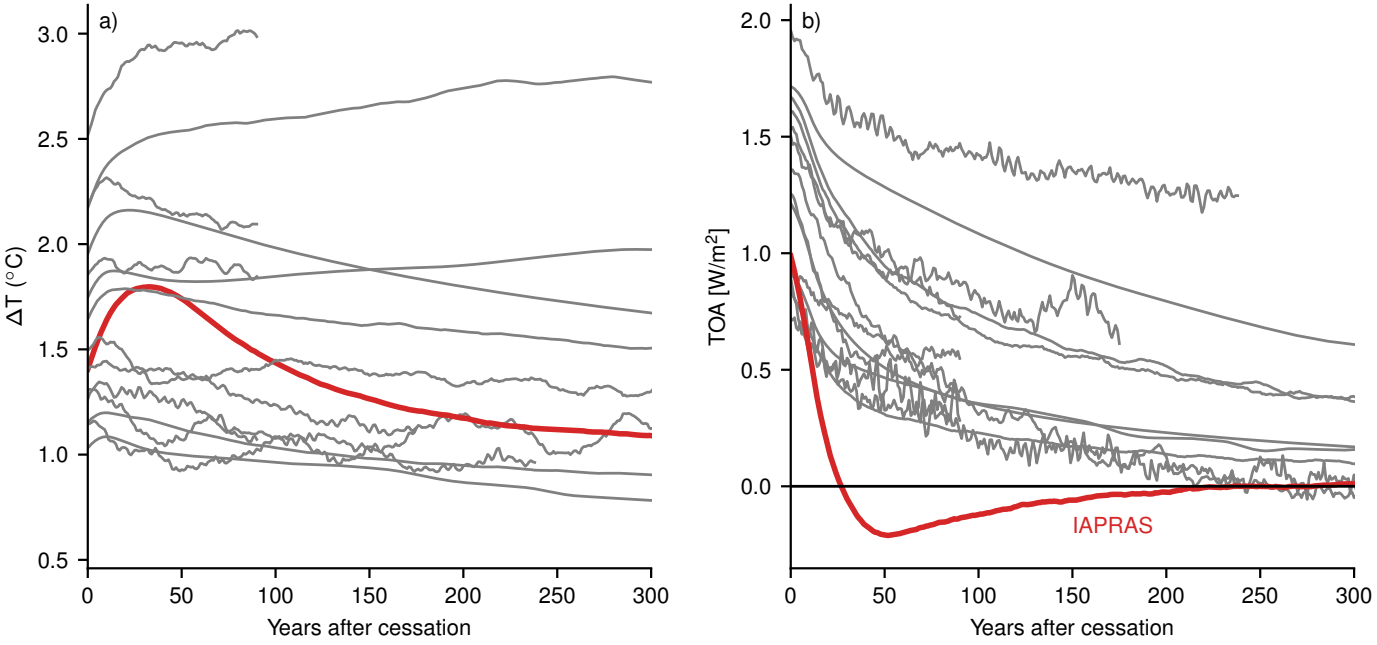

Supplementary Fig. 5 Temperature anomaly and top-of-atmosphere radiative imbalance (TOA) in IAPRAS compared to other ZECMIP models. Data corresponds to post-emissions evolution in the ZECMIP A1 experiment [10], which follows a 1%/yr growth in the CO_2 concentration until diagonsed cumulative emissions equal 1000 GtC, at which time emissions cease. Results are smoothed with a 20-year, centered average. IAPRAS is the only model to exhibit a sharp reversal in the sign of the TOA imbalance shortly after emissions cessation and substantial non-monotinicity in the temperature response.

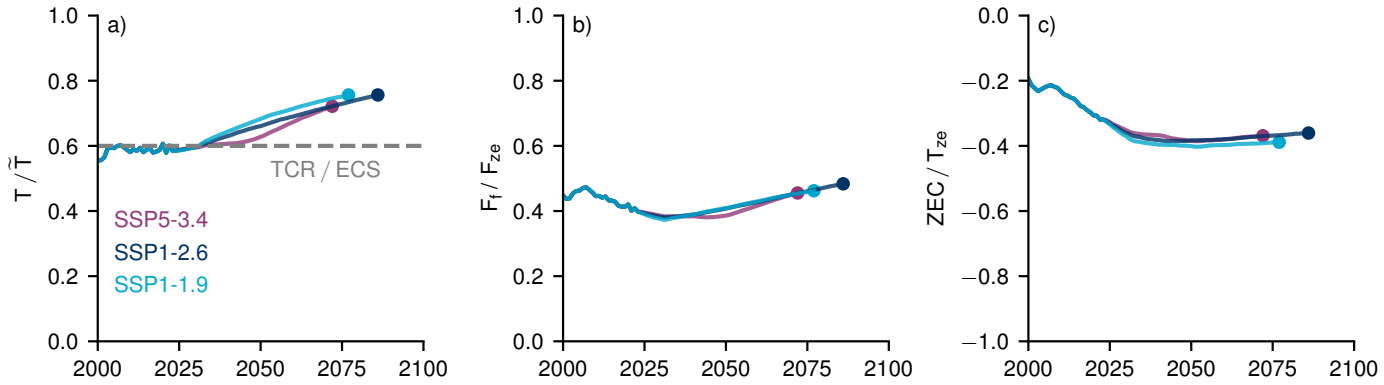

Supplementary Fig. 6 Evolution of disequilibria and ZEC in the net-zero SSPs. FaIR model results for the thermal disequilibrium (a), forcing disequilibrium (b), and the fractional change in ZEC (c) for the SSPs that achieve net-zero GHG (circles) this century.

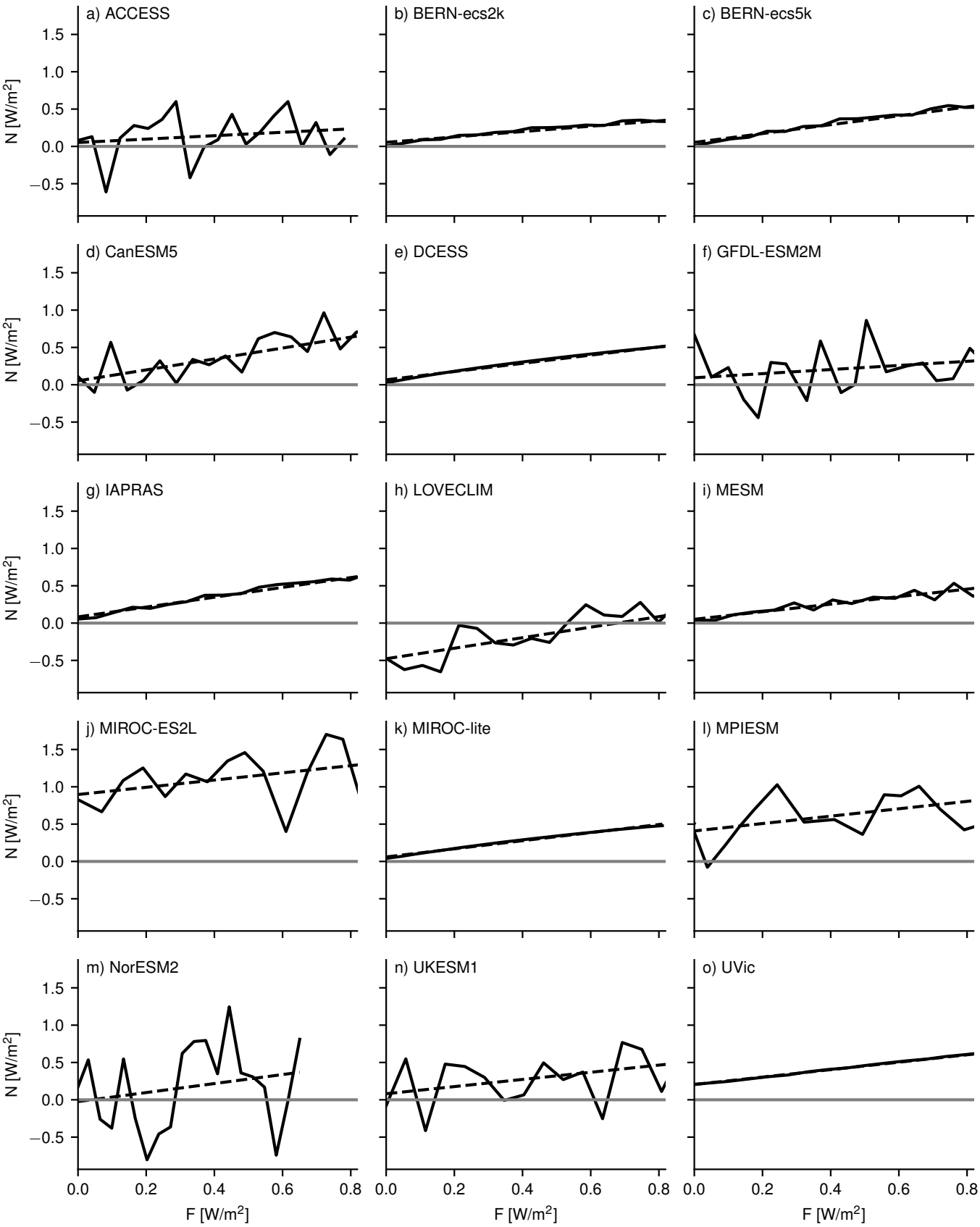

Supplementary Fig. 7 Initial energy imbalance in ZECMIP models. The top-of-the-atmosphere energy imbalance N versus the radiative forcing for ZECMIP models over the first 20 years of the 1%/yr CO_2 experiments. Linear regression (dotted) is performed to estimate the pre-industrial N, which may be non-zero due to energy conservation error or insufficient spin-up time.

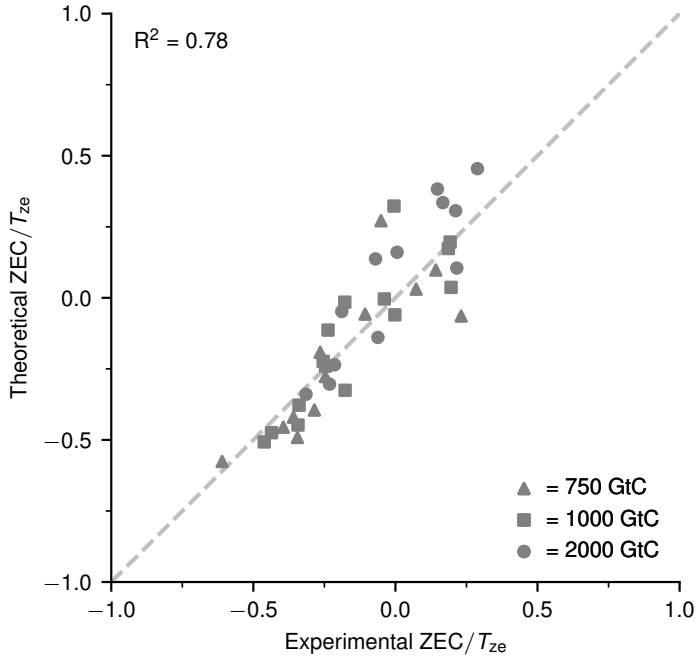

Supplementary Fig. 8 Theory compared to all ZECMIP experiments. Comparison between the analytic formula (Eqn. 4) and the experimental values for the fractional change after emissions cessation following a 1%/yr increase in CO_2 up to 750 (triangles), 1000 GtC (squares), and 2000 GtC (circles) in the ZECMIP ensemble.

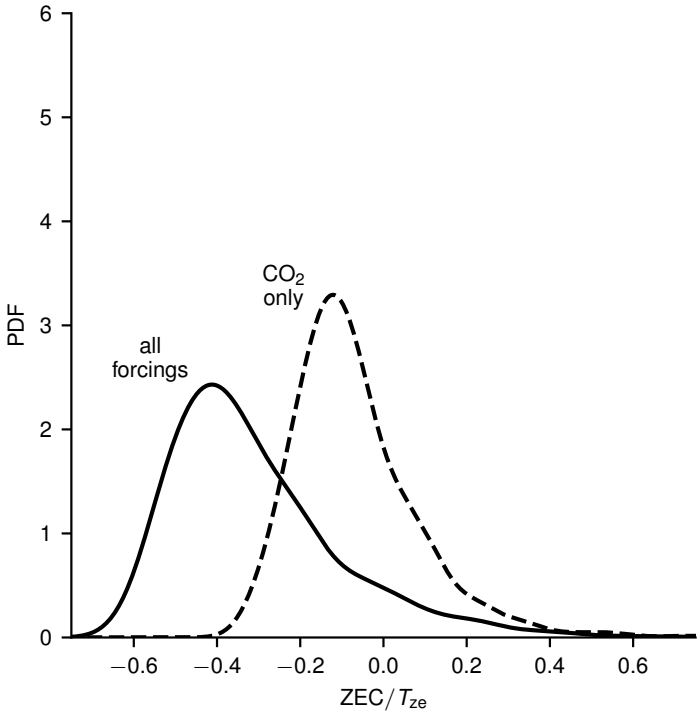

Supplementary Fig. 9 Non-CO_2 forcings lower ZEC. The probability density function (PDF) for ZEC/T_{ze} resulting from driving the FaIR ensemble with all forcings (solid curve) versus only CO_2 (dashed curve) up to present-day (2024) followed by emissions cessation. PDFs are kernel density estimates with bandwidths set by Silverman's rule [27].

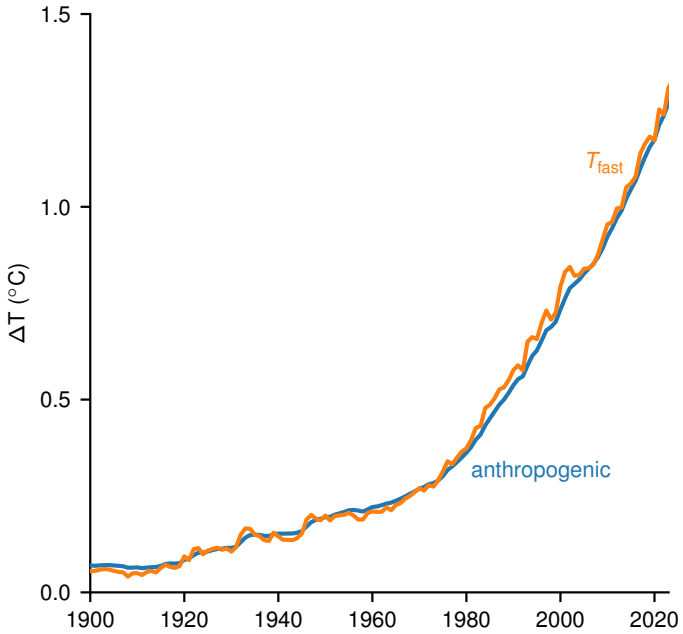

Supplementary Fig. 10 Anthropogenic component of historical temperature rise explained by fast mode. The median temperature response of the FaIR ensemble (blue) when driven by only anthropogenic forcing compared to the fast-mode solution: $T_{\text{fast}} = \text{TCR}\,(F/F_{2x})$.

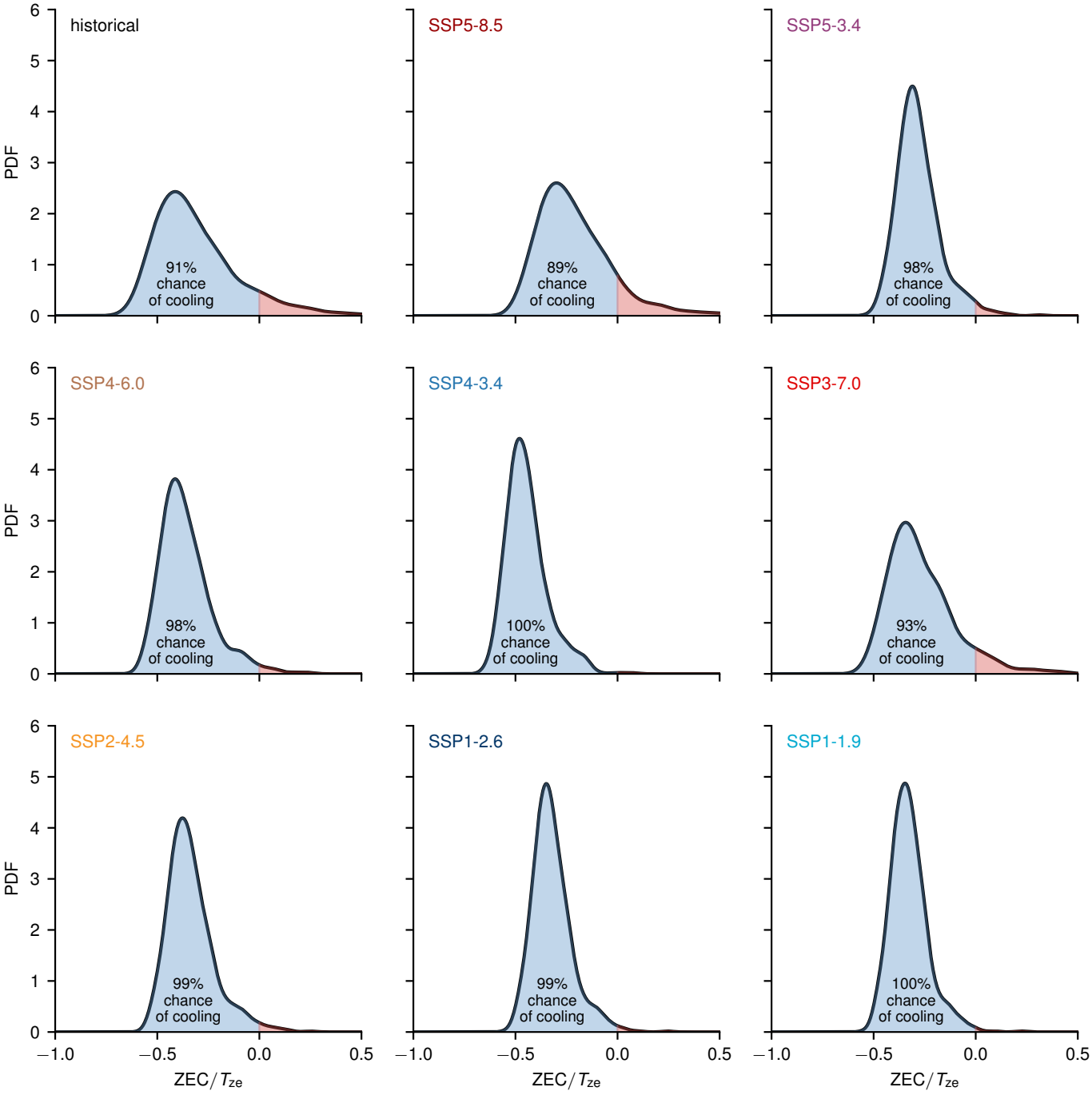

Supplementary Fig. 11 ZEC distributions in the SSPs. The probability-density functions for the FaIR ensemble given SSP emissions up to 2100, after which emissions cease.

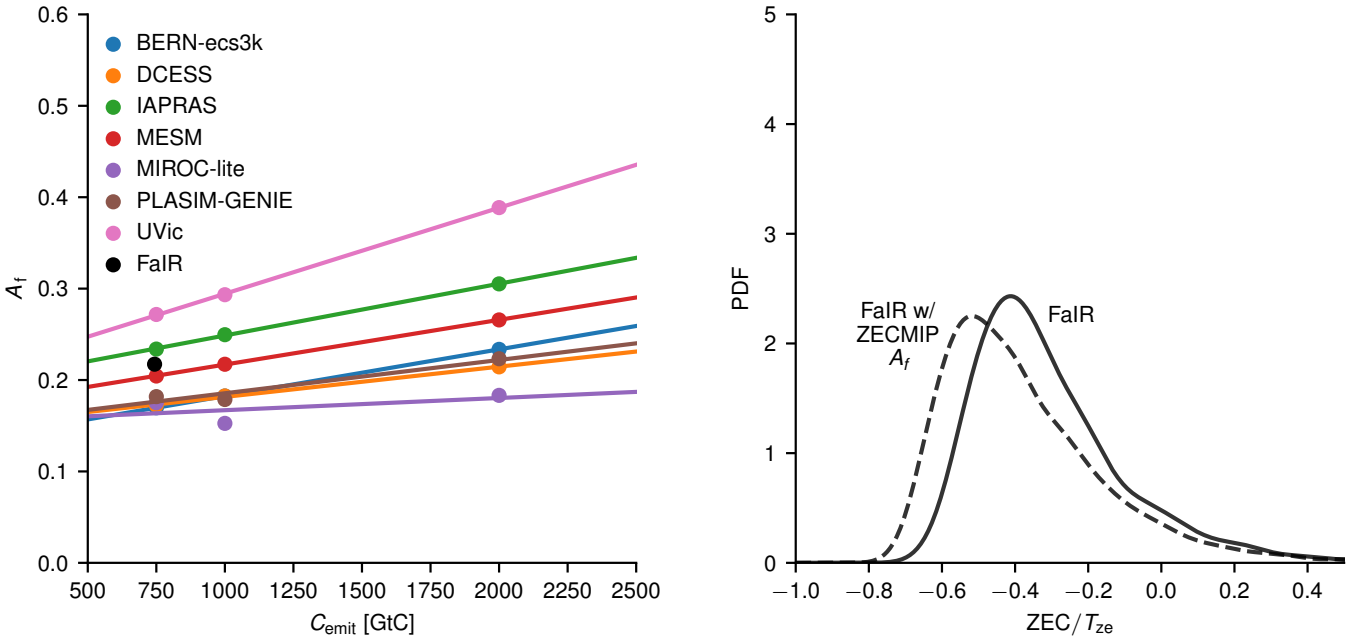

Supplementary Fig. 12 ZECMIP A_f results and their implications for ZEC/T_{ze}. *Left:* Final airborne fraction (A_f) in the millennial ZECMIP experiments for cumulative CO_2 emissions of 750, 1000, and 2000 GtC. Per-model linear fits (via least-squares regression) are also shown. The black marker indicates the final A_f from FaIR, which is larger than that of most ZECMIP models. *Right:* Probability density functions (PDFs) for historical ZEC/T_{ze} (i.e., the relative temperature change given no future emissions). The solid line shows results using FaIR's default A_f, while the dotted line results from substituting FaIR's A_f with the ZECMIP results. In this case, for each ZECMIP model, we use the per-model linear fits to find A_f for historical emissions, then recalculate the FaIR ensemble's predictions given that A_f. Results for all ZECMIP models are combined into an ensemble of size 7×841, whose PDF is shown by the dotted curve. Because the average ZECMIP model has a smaller A_f than FaIR's default, this PDF is shifted toward greater cooling relative to the default FaIR ensemble.

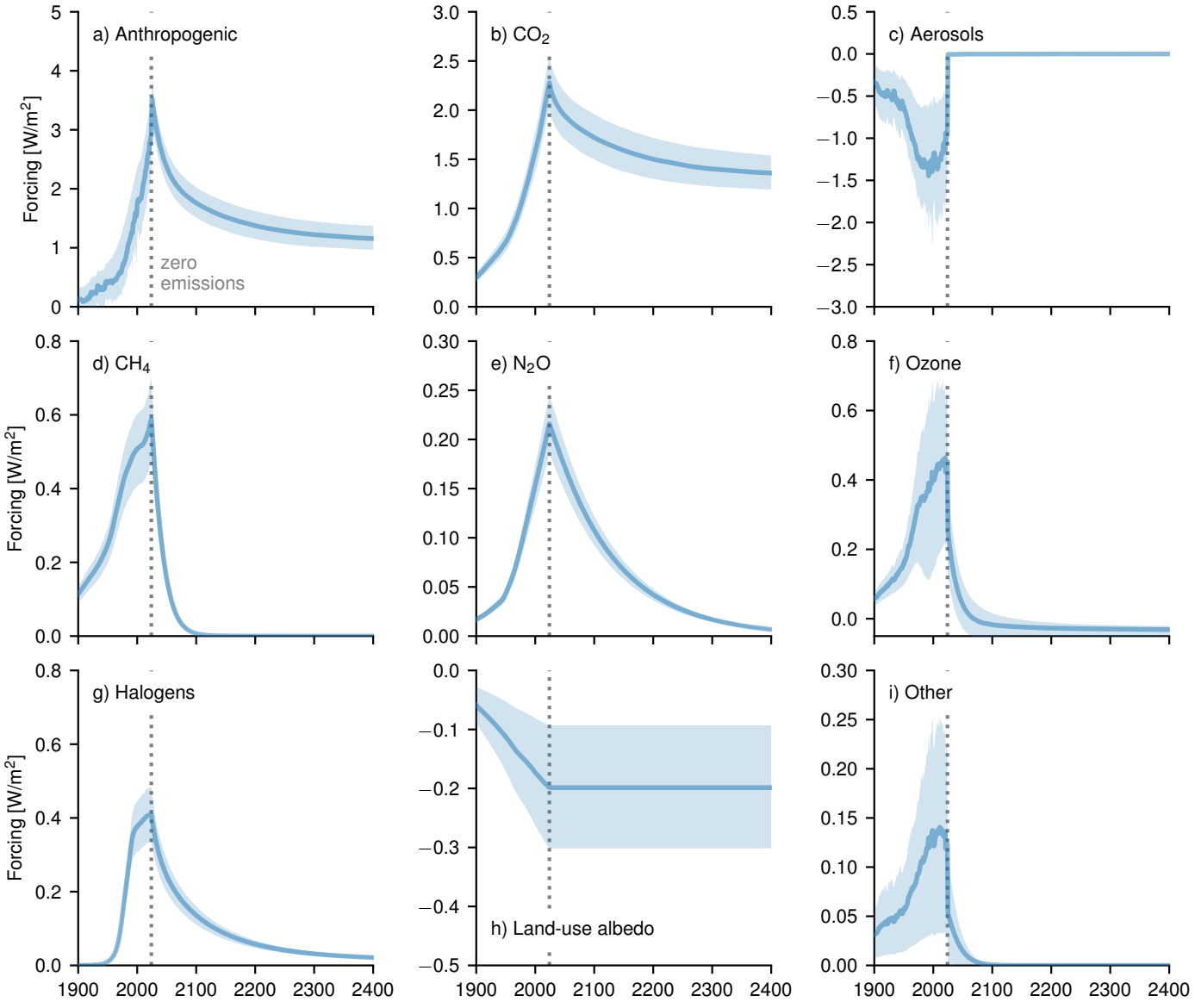

Supplementary Fig. 13 Anthropogenic ERF absent future emissions. ERF computed in the FaIR ensemble driven by historical emissions and no future emissions (i.e., the historical ZEC experiment). Shading shows the 5th-95th interquantile range.